



Published in final edited form as:

J Med Chem. 2012 September 13; 55(17): 7425–7436. doi:10.1021/jm300351w.

Bioisosteric transformations and permutations in the triazolopyrimidine scaffold to identify the minimum pharmacophore required for inhibitory activity against *Plasmodium falciparum* dihydroorotate dehydrogenase

Alka Marwaha¹, John White¹, Farah El_Mazouni², Sharon A Creason³, Sreekanth Kokkonda¹, Frederick S. Buckner³, Susan A. Charman⁴, Margaret A. Phillips^{2,*}, and Pradipsinh K. Rathod^{1,*}

¹Department of Chemistry and Global Health, University of Washington, Seattle, WA 98195

²Department of Pharmacology, University of Texas Southwestern Medical Center at Dallas, 6001 Forest Park Rd, Dallas, Texas 75390-9041

³Department of Medicine, University of Washington, Seattle, WA 98195

⁴Centre for Drug Candidate Optimisation, Monash Institute of Pharmaceutical Sciences, Monash University (Parkville campus), Parkville, VIC 3052, Australia

Abstract

Plasmodium falciparum causes approximately 1 million deaths annually. However increasing resistance imposes a continuous threat to existing drug therapies. We previously reported a number of potent and selective triazolopyrimidine-based inhibitors of *Plasmodium falciparum* dihydroorotate dehydrogenase that inhibit parasite *in vitro* growth with similar activity. Lead optimization of this series led to the recent identification of a preclinical candidate, showing good activity against *P. falciparum* in mice. As part of a backup program around this scaffold, we explored heteroatom rearrangement and substitution in the triazolopyrimidine ring and have identified several other ring configurations that are active as *PDHODH* inhibitors. The imidazo[1,2- α]pyrimidines were shown to bind somewhat more potently than the triazolopyrimidines depending on the nature of the amino aniline substitution. **DSM151**, the best candidate in this series, binds with 4-fold better affinity (*PDHODH* IC₅₀ = 0.077 μ M) than the equivalent triazolopyrimidine and suppresses parasites *in vivo* in the *P. berghei* model.

Introduction

Malaria is a persistent and successful global disease that threatens half of the world's population and kills up to a million people each year.^{1, 2} The developing world has urgently needed new, safe, effective and affordable antimalarial drugs since the demise of chloroquine due to the emergence of resistant *P. falciparum* strains.^{3, 4} Strides have been made to develop an array of anti-malarial agents with Artemisinin-based combination therapies (ACTs) providing a major breakthrough, succeeding in more than 90% of the malaria cases.^{5–8} However, artemisinin effectiveness appears to be decreasing along Thai-Cambodia border threatening these recent gains.^{9, 10} The limitations of current antimalarial

*Corresponding Author Rathod, telephone, 206-221-6069; fax, 206-685-8665; rathod@chem.washington.edu; Phillips, telephone, 214-645-6164; fax, 214-645-6166, Margaret.Phillips@UTSouthwestern.edu.

The authors declare no competing financial interest.

chemotherapy underscore the need for novel drugs, ideally directed against innovative therapeutic targets. The completion of the malaria genome project¹¹ has opened up channels to search for new targets in the parasite. Despite the identification of many essential genes and extensive efforts to understand the biology of the parasite, very few unique validated targets have been identified. Hence, the contemporary challenge is to blend our knowledge of malaria genomics and drug discovery.

Nucleic acid biosynthesis in *P. falciparum* differs from that in mammals. The parasite relies on purine salvage due to the absence of *de novo* purine synthesis^{12–15}. The situation is reversed for pyrimidine biosynthesis where the parasite lacks salvage enzymes for preformed pyrimidine bases and nucleosides, and thus relies on the *de novo* biosynthesis. *Plasmodium falciparum* dihydroorotate dehydrogenase (*PfDHODH*), an essential mitochondrial flavin mononucleotide-dependent enzyme, catalyzes the fourth and rate-limiting step in *de novo* pyrimidine biosynthesis.^{16, 17} Recent investigations have revealed that the primary task of the mitochondrial electron transport chain in the parasite is to supply oxidized ubiquinone (CoQ) to DHODH for pyrimidine synthesis, confirming the essential role of DHODH in parasite growth.¹⁸ The efficacy of human DHODH inhibitors for the treatment of rheumatoid arthritis has been well-documented in the literature, demonstrating that DHODH is a druggable target.^{19–21} Finally, X-ray structures of *hDHODH* and *Plasmodium* DHODH have highlighted an extensive variation in amino acid sequence between the human and malarial enzymes,^{22–25} thereby, providing the structural basis for the identification of species-specific inhibitors.

A high-throughput screen (HTS) of “drug-like” small molecules, using a colorimetric enzyme assay, led to the identification of a highly potent and selective triazolopyrimidine-based *PfDHODH* inhibitor **1** (DSM 1, Figure 1), (5-methyl-[1,2,4]triazolo[1,5-*a*]pyrimidin-7-yl)naphthalene-2-ylamine.^{26–28} **1** has potent activity against both *PfDHODH* (IC₅₀ = 0.047 μM) and *P. falciparum* parasites in whole cell assays (EC₅₀ = 0.079 μM for clone 3D7), without inhibiting human DHODH. However when administered orally to mice infected with *P. berghei*, **1** had no anti-parasite activity. The lack of efficacy of **1** was traced to rapid and possible induced metabolism and to species differences in inhibitor potency between *PfDHODH* and *Plasmodium berghei* dihydroorotate dehydrogenase (*PbDHODH*).²⁹ An integrated lead optimization program combining medicinal chemistry, enzymology and pharmacologic evaluation was utilized to identify a modified analog **2** (DSM 74, Figure 1), 5-methyl-*N*-(4-(trifluoromethyl)phenyl)-[1,2,4]triazolo[1,5-*a*]pyrimidin-7-amine, with greater metabolic stability. This compound showed good exposure *in vivo* after oral dosing and was able to suppress parasitemia in the *P. berghei* model.²⁹ However, **2** lacked the potency required of a clinical candidate. Subsequent X-ray structure guided lead optimization of the scaffold identified **3** (DSM265, Figure 1), 2-(1,1-difluoroethyl)-5-methyl-*N*-[4-(pentafluoro-λ⁶-sulfanyl)phenyl]-[1,2,4]triazolo[1,5-*a*]pyrimidin-7-amine, which is a potent inhibitor of *PfDHODH* that is able to kill parasites *in vitro* and showed efficacy in a rodent model similar to chloroquine.^{30, 31} **3** is also metabolically stable and exhibits a long half-life after oral administration in rodents. Based on these strengths **3** has recently been selected as a preclinical drug development candidate.

As part of our back up program to identify additional compounds with clinical candidate potential we extended our explorations of the triazolopyrimidine scaffold by applying bioisosteric morphing, a hit optimization strategy to replace the core of a bioactive compound with groups of similar physical or chemical properties without loss of activity. Using this strategy we have synthesized a series of compounds with either modified bridging atoms between the triazolopyrimidine ring and the aromatic moiety (**4–5**, Figure 2) or heteroatom rearrangements/replacements in the triazolopyrimidine ring (**6–11**, Figure 3). We initially coupled each new ring system to naphthyl amine (as in **1**), but then for active

scaffolds we tested some additional aryl amines (**12** – **16**) to determine if the optimal group in this position remained similar to what we have observed for the triazolopyrimidines. Three additional heteroatom ring configurations were identified that showed submicromolar *PfDHODH* activity (**6**, **7** and **9**), with the best being the imidazo[1,2-*a*]pyrimidines (**6** and **16**, Table 1) having equivalent to more potent binding affinity compared to the matched triazolopyrimidine. The imidazo[1,2-*a*]pyrimidine **16** was chosen for profiling of its *in vivo* properties, including pharmacokinetic analysis and efficacy testing in the *P. berghei* mouse model. Plasma exposure was lower than for the matched triazolopyrimidine, leading to reduced efficacy. The *in vitro* metabolism data suggested that the imidazo[1,2-*a*]pyrimidine scaffold is more extensively metabolized than the triazolopyrimidine scaffold in mice, suggesting additional chemistry would be required to exploit the activity of this scaffold. These studies have provided important additional insight into the developing structure activity relationships (SAR) in this promising series of anti-malarial compounds.

Chemistry

Amide mimics

In order to test the effects of modifying the linker between the triazolopyrimidine ring and the naphthyl group, the bridging nitrogen N1 was replaced with an amide linker (Figure 2). The target inhibitors **4**–**5** were synthesized *via* a three-step sequence as depicted in Scheme 1. The first two steps were relatively straightforward, based on our reported protocol.²⁹ Our initial attempts to perform the coupling reactions of amides with the key intermediate 7-chloro-5-methyl-[1,2,4]triazolo[1,5-*a*]pyrimidine (**17**), using traditional conditions like stirring at ambient temperature in absolute ethanol with or without the *p/o* base, refluxing in toluene, refluxing in absolute ethanol/dichloromethane/*N,N*-dimethyl formamide, with and without the *p/o* bases like triethyl amine /anhydrous potassium carbonate, were unsuccessful and rather afforded either the hydroxy-derivative or the ethoxy substituted products. In order to establish a robust synthetic procedure for the targets, the reaction conditions were judiciously optimized using transition metal catalyzed Buchwald-Hartwig conditions.^{32–35}

We tried few combinations of 2,2'-bis(diphenylphosphino)-1,1'-binaphthyl (BINAP) as ligand, Pd(OAc)₂ as a source of palladium and different reaction variables to determine the efficient catalytic system and found the amidation coupling was optimal using a Pd(OAc)₂ (5 mol %)/BINAP (5 mol %) combination, sodium *tertiary* butoxide (5 molar equivalents) as base. Other stoichiometric bases like potassium carbonate or cesium carbonate worked less well both in terms of yields and reaction progress up to completion. A large excess of base, though almost insoluble in toluene, was essential to obtain high cross-coupling rates with dry toluene as solvent.

The reaction progress was monitored by MS and TLC screening. From a complex reaction mixture, the desired cross-coupled products **4**–**5** were isolated in optimal yields (40–50%) after silica gel column chromatographic purification.

Heteroatom ring rearrangements and replacements

In order to explore the SAR of the triazolopyrimidine core, we synthesized a series of derivatives to test if the heteroatoms (nitrogens) could be replaced with carbon, resulting in the corresponding heteroaromatic rings with comparable steric and electronic characteristics (Figure 3a–c). Our prime interest was the systematic evaluation of the effects of removal of individual nitrogen atoms from the triazolopyrimidine core to construct imidazo[1,2-*a*]pyrimidines (**6**), triazolo[1,5-*a*]pyridine (**7**) and pyrazolo[1,5-*a*]pyrimidine (**8**) ring systems (Figure 3b), which were further extended to the related congeneric purines (**9**), pyrazolo[3,4-

d]pyrimidine (**10**) and triazolo[4,3-*a*]pyridazine (**11**) (Figure 3c). Herein we report our approaches on the synthesis of these various bioisosteres.

Scaffold hops 6–16

The imidazo[1,2-*a*]pyrimidine analogs (**6** & **16**) were readily synthesized as depicted in Scheme 2. The commercially available 2-amino-imidazole hemisulfate (**19a**) was condensed with ethyl acetoacetate in refluxing glacial acetic acid to afford 5-hydroxy-7-methylimidazo[1,2-*a*]pyrimidine (**20a**).³⁶ Chlorination of **20a** using phosphorus oxychloride gave the intermediate 5-chloro-7-methylimidazo[1,2-*a*]pyrimidine (**21a**). Final conjugation of **21a** with 2-aminonaphthalene and 4-(trifluoromethyl)aniline afforded **6** and **16**, respectively.

The target inhibitor **7** was obtained by coupling 5-chloro-7-methyl-[1,2,4]triazolo[1,5-*a*]pyridine (**18**, commercially available) with 2-aminonaphthalene utilizing transition-metal catalyzed conditions (Scheme 1).

Compound **8** was prepared as outlined in Scheme 2. A mixture of 1*H*-pyrazol-5-amine (**19b**) and ethyl acetoacetate was refluxed in glacial acetic acid to yield, 7-hydroxy-5-methylpyrazolo[1,5-*a*]pyrimidine (**20b**). Subsequent chlorination^{37, 38} (**21b**) and coupling with 2-amino naphthalene (Scheme 2) afforded the final adduct **8**.

The congeners **9**, **10**, **11** and **12–15** were prepared as depicted in the Scheme 2 & 3. Regarding purine analogs **9** and **12–15**, condensation of 4-amino-1*H*-imidazole-5-carboxamide hydrochloride salt (**22a**) with triethyl orthoacetate in refluxing anhydrous dimethylformamide^{39–41} afforded 4-(methylethoxymethylene)-aminoimidazole-5-carboxamide (**23a**), which was then cyclized intramolecularly at elevated temperatures to give 2-methylhypoxanthine (**24a**). Ensuing chlorination and coupling of **25a** with variously substituted aromatic amines afforded **9** and **12–15**.

Pyrazolo[3,4-*d*]pyrimidine (**10**) was synthesized from 5-amino-1*H*-pyrazole-4-carboxamide hemisulfate (**22b**) as delineated in Scheme 3. Refluxing **22b** with triethyl orthoacetate in anhydrous DMF afforded 5-(methylethoxymethylene)-aminopyrazole-4-carboxamide (**23b**), intramolecular cyclization of which at elevated temperature yielded 4-hydroxy-6-methyl-1*H*-pyrazolo[3,4-*d*]pyrimidine (**24b**). Subsequent chlorination⁴² and coupling with 2-amino-naphthalene afforded **10**.

The triazolopyridazine **11** was synthesized using the reaction sequence highlighted in Scheme 2. 4-amino-1,2,4-triazole (**19c**) interacted with ethyl acetoacetate in refluxing glacial acetic acid to produce 8-hydroxy-6-methyl-[1,2,4]triazolo[4,3-*b*]pyridazine (**20c**), which on chlorination using phosphorus oxychloride, afforded 8-chloro-6-methyl-[1,2,4]triazolo[4,3-*b*]pyridazine (**21c**).⁴³ Various conditions using a variety of solvents, bases and temperatures were attempted and found unsuccessful. However, the reaction conditions were optimized utilizing transition metal-catalysis. As previously described (for inhibitors **4–5**, Scheme 1), the catalytic combination of Pd(OAc)₂ (5 mol%)/BINAP (5 mol %) was found to work well with sodium *tertiary* butoxide (5 molar equivalents) as base and anhydrous toluene as the solvent (Scheme 2). The reaction temperature and the reaction time were 120 °C and 24 h.

Results and Discussion

Evaluation of compound activity against DHODH and *P. falciparum* 3D7 cells

The functional evaluation of the target inhibitors **4–16** was carried out on the parasite and host DHODH and on *P. falciparum* 3D7 cells in whole cell assays (Table 1). The

compounds showed a wide range of IC₅₀ values against *PfDHODH* (0.077 - >100 μM) and these values showed a good correlation with activity against *P. falciparum* 3D7 cells (Table 1 and Figure 4). All compounds tested were inactive against human DHODH, showing that the selectivity of the series was maintained by variations in the triazolopyrimidine ring. Most compounds also showed better activity against *PfDHODH* than *P. berghei* DHODH, similar to previous reports for the series.^{27, 29, 31, 44} We deduce the following SAR trends by comparing the activity of these compounds against the previously described triazolopyrimidines **1** and **2**.

1. Replacement of the –NH linker with amide –NHCO (**4** and **5**) resulted in the loss of activity when an aniline or substituted aniline was adjacent to the amide bond.
2. Replacement of triazolopyrimidine core with imidazo[1,2-*a*]pyrimidine was well tolerated, and either slightly reduced or slightly enhanced binding affinity depending on the nature of the aromatic amine. **6** was 3-fold less potent than **1** (IC₅₀ = 0.15 μM vs 0.047 μM), but **16** was 4-fold more potent than **2**.
3. Replacement of the triazolopyrimidine core with triazolo[1,5-*a*]pyridine (**7**) resulted in a 100-fold reduction in binding affinity, thereby showing that the pyrimidine nitrogen N5 plays a pivotal role in the observed activity of the triazolopyrimidines.
4. Substitution of the core with pyrazolo-[1,5-*a*]pyrimidine (**8**) reduced the activity by ~ 8.5-fold demonstrating the importance of the N4 nitrogen in the five-membered ring to both the enzyme inhibition and anti parasitic activity.
5. The purine analog **9** involving bioisosteric replacements at two sites was ~ 9-fold less active than the comparable triazolopyrimidine compound. Additional derivatives of this scaffold were also evaluated by replacing the naphthyl group with anthracene, quinoline, isoquinoline and substituted five-membered pyrazole rings (**12**, **13**, **14** and **15**). Exchange of naphthyl with larger moiety like anthracene (**12**) considerably lessened the activity (~ 87-fold), which is in contrast to what was observed for this replacement in the triazolopyrimidine core structure.²⁹ Further, incorporation of heteroatoms in the naphthyl system (**13** and **14**) reduced the activity as was previously observed for the triazolopyrimidine scaffold.²⁹ The five-membered 4-cyanopyrazole (**15**) was inactive.
6. Bioisosteric modification involving four changes in the purine related analogs i.e. pyrazolo[3,4-*d*]pyrimidine **10** and triazolopyridazine **11** inactivated the compound.
7. Loss of N2 in analogs **9**, **10** and **11** is also correlated to a significant reduction in activity, suggesting that N2 may also be important to the potency of the compound class. However in all cases these compounds also contained an additional nitrogen in a position not found in the triazolopyrimidines so conformation of the role of N2 through additional synthesis is still required.

Structural basis of activity differences between the triazolopyrimidines and variations in the core

The X-ray structure of key triazolopyrimidine *PfDHODH* inhibitors, including **1** and **2**, was previously reported by our group.²³ These structures showed that the triazolopyrimidine ring forms a H-bond interaction between the pyrimidine nitrogen N5 and R265, and between the bridging nitrogen N1 and H185 (Figure 5). These are the only polar interactions formed between the inhibitor and the enzyme, and site-directed mutagenesis confirmed that both interactions were essential for high affinity binding of these compounds. Analysis of the structures described in this manuscript further confirms the importance of these interactions.

Compound **7**, in which the pyridine nitrogen N5 is replaced with carbon is 100-fold less potent than the corresponding triazolopyrimidine (**1**), demonstrating that the interaction between the pyrimidine nitrogen N5 and R265 is essential for high affinity binding. In prior studies we noted that introduction of heteratoms into the naphthyl ring reduced activity for the triazolopyrimidine series.^{26,27} This result holds true for the purine analogs (**14** and **15** compared to **9**), and is explained by the X-ray structure that shows the naphthyl pocket is completely hydrophobic with no potential to contribute to H-bond interactions. Finally, the structure also provides insight into the good activity of the imidazo[1,2-*a*]pyrimidines **6** and **16**. Nitrogen N3 is within 3.3 Å of NE1 of H185, yet this interaction cannot be productive because NE1 of H185 is an H-bond acceptor and not an H-bond donor. Replacement of N3 with carbon may thus relieve a potentially negative interaction between these groups. It also may lead to the displacement of the structural water observed to form H-bond interactions with N3, H185 and Y525. The entropic gain in releasing the water could also contribute to greater binding affinity of **16** relative to **2**. It is unclear why the effect of removing N3 on improving potency was only evident when the imidazo[1,2-*a*]pyrimidine core was coupled with the smaller para-CF₃ aniline and not when it was coupled to naphthyl amine (**1** vs **6**). This data suggests that the relative contribution of N3 to the electronics of the ring differs depending on the coupled aromatic amine, and that considerations beyond H-bond potential and displacement of the bound water play roles in the potency of these compounds.

In vitro metabolic stability and PK in mice

The most active compound in the present series **16** was advanced to metabolism and *in vivo* studies. *In vitro* metabolic analysis in human liver microsomes for **16** was compared to previous results collected for **2**. Both **2** and **16** display low *in vitro* intrinsic clearance values (E_h) in human liver microsomes, but **16** displayed intermediate clearance in mouse microsomes suggesting that plasma exposure in mice might limit the ability of the compound to show good *in vivo* efficacy (Table 2). The reason **16** displays higher *in vitro* intrinsic clearance than **2** is unknown. To evaluate the pharmacokinetic profile of **16**, mice were dosed orally with **16** at a single dose of 10 mg/kg (Figure 6A). **16** reached peak plasma concentrations of 3.9 μM after oral dosing, but plasma levels were maintained above 1 μM for only about 4 h and by 16 h concentrations were below the limit of quantitation (0.003 μM). No adverse reactions were observed following oral administration of **16** at the dose used in this study.

In vivo efficacy of **16** in *P. berghei* mouse model

16 was evaluated for efficacy in the standard *P. berghei* mouse model. Mice were infected with *P. berghei* on day zero and dosing began 24 h after infection. Mice were dosed orally with 50 mg/kg **16**, 1× daily for 4 days, and parasite blood levels were evaluated and compared to a chloroquine control (Figure 6B). **16** suppressed parasite levels by 56% as measured 24 h after the final dose. In comparison **2** was able to suppress parasite levels by 71% using the same dosing scheme and end point.²⁹ Thus despite showing 2-4-fold better potency against *PbdHODH* and *PdHODH* than **2** respectively, **16** is less efficacious than **2** in the mouse model. The relatively poorer plasma exposure observed in mice for **16** most likely contributes to this finding. The finding that the predicted *in vitro* clearance in mouse microsomes is significantly higher than human microsomes suggests that this compound would perform better against human infection than for mice.

Conclusion—In the quest for better *PdHODH* antagonists, we have undertaken a study to systematically explore the importance of the number and configuration of nitrogen atoms in the triazolopyrimidine ring to the potency of the compound class. The studies show that N1, N4 and N5 are functionally important sites as the structural modification at these positions

render the molecule less or completely inactive (Figure 7). N3 can be replaced by carbon leading to retained or improved potency; however the N3 nitrogen is a significant factor in the metabolic stability and favorable pharmacokinetics of **2**. In particular, **16** was found to be 4-fold more potent than the equivalent triazolopyrimidine **2**, however the poorer plasma exposure led to reduced efficacy against the parasite *in vivo*. The addition of an amide linker between the triazolopyrimidine core and the aniline also led to complete loss of activity. Overall the data have helped to define the minimal pharmacophore of the triazolopyrimidine class of *PfDHODH* inhibitors, and have highlighted the key importance of the pyrimidine nitrogen N5.

Experimental

Protein purification and steady-state kinetic analysis

PfDHODH, *PbDHODH*, and *hDHODH* enzymes were expressed and purified as previously reported.^{27, 28, 45} Steady-state kinetic assays were performed as previously described.^{27, 28, 45} Briefly, this colorimetric assay monitors the reduction of 2,6-dichloroindophenol (DCIP; 0.12 mM) at 600 nm ($\epsilon = 18.8 \text{ mM}^{-1}\text{cm}^{-1}$), which is coupled to the reoxidation of CoQ_D (coenzyme Q_D). The assay was carried out using a solution containing 100 mM HEPES, pH 8.0, 150 mM NaCl, 10 % Glycerol, 0.1 % Triton X-100, 20 micromolar CoQ_D, 200 micromolar L-dihydroorotate and 120 micromolar DCIP. Reactions were initiated by addition of enzyme to a final concentration in the range of 5–10 nM while maintaining the temperature of the circulating water bath at 20 °C. The data obtained were fitted to Eq 1 using GraphPad Prism, to determine the IC₅₀ values of the representative compounds. IC₅₀ data were determined over a range of inhibitor concentrations using triplicate data points at each concentration and errors represent the standard error of the fit.

$$v_i = \frac{v_0}{1 + \frac{[I]}{IC_{50}}} \quad \text{Eq.1}$$

P. falciparum cell culture

The malarial parasite clone 3D7 was passaged in Gibco-Invitrogen RPMI-1640 supplemented with 20% human type A+ plasma and 2% (w/v) red blood cells (obtained from Biochemed Services, Virginia).⁴⁶ To study inhibition of cell proliferation, the standard [³H]-hypoxanthine uptake assay was used to measure drug-treated *P. falciparum*-infected-erythrocytes as described previously.⁴⁷ Data were fitted to Eq. 2 to determine EC₅₀ (n = 3 – 4 data points at each concentration). Since the standard error of the fit cannot be calculated for Eq. 2, the parasite data is reported with the 95% confidence interval from the fit.

$$\%CellProliferation = \frac{100\%}{1 + 10^{(\log EC_{50} - \log [I])HillSlope}} \quad \text{Eq.2}$$

In vitro human microsomal metabolism

Metabolic stability was evaluated by incubating test compounds (1 μM) individually at 37°C with pooled human or mouse liver microsomes (BD Gentest, Woburn, MA) at a microsomal protein concentration of 0.4 mg/mL. The metabolic reaction was initiated by the addition of an NADPH-regenerating buffer system containing 1 mg/mL NADP, 1 mg/mL glucose-6-phosphate, 1 U/mL glucose-6-phosphate dehydrogenase and 0.67 mg/mL MgCl₂, and reactions were quenched at various time points over the incubation period by the addition of ice-cold acetonitrile. The relative loss of parent compound and formation of

metabolic products was monitored by LC/MS using a Waters/Micromass QTOF mass spectrometer.

Test compound concentrations were determined by comparison to a calibration curve prepared in microsomal matrix and concentration versus time data were fitted to an exponential decay function to determine the first-order rate constant for substrate depletion. This rate constant was then used to calculate the degradation half-life, *in vitro* intrinsic clearance ($CL_{int, in vitro}$), predicted *in vivo* intrinsic clearance value (CL_{int}), and predicted *in vivo* hepatic extraction ratio (E_H) as previously described,⁴⁸ and assuming predominantly hepatic cytochrome P450-mediated clearance *in vivo*. The scaling parameters used in these calculations included a human and mouse hepatic blood flow of 20.7 and 90 mL/min/kg, respectively, liver mass of 25.7 and 87.5 g liver/kg body weight for human and mouse, respectively, and microsomal content of 45 mg microsomal protein/g liver.^{49, 50}

Mouse pharmacokinetics

All animal studies were performed in accordance with the Australian and New Zealand Council for the Care of Animals in Research and Training Guidelines and the study protocol was approved by the Monash University (Victorian College of Pharmacy) Animal Experimentation Ethics Committee. The pharmacokinetics of **16** were studied in non-fasted male Swiss outbred mice weighing 23–33 g. Mice had access to food and water *ad libitum* throughout the pre- and post-dose sampling period. Compound was administered orally by gavage (0.1 mL dose volume per mouse) in a suspension of aqueous vehicle (0.5% w/v sodium caboxymethylcellulose, 0.5% v/v benzyl alcohol and 0.4% v/v Tween 80). Samples were collected at 1, 2, 4, 7.5, 16 and 24 h post-dosing with a single blood sample from each mouse via cardiac puncture. Blood samples were transferred to heparinised tubes, centrifuged immediately, and supernatant plasma removed and stored at –20°C until analysis (within 1–2 weeks). Plasma samples were assayed by LC-MS following protein precipitation with acetonitrile and the concentration of drug in plasma was determined by comparison of the peak area to a calibration curve prepared in plasma.

P. berghei mouse in vivo efficacy testing

All animal care and experimental procedures were approved by the Institutional Animal Care and Use Committee at the University of Washington. Eight to ten week old female BALB/c mice were obtained from Jackson Laboratories (Bar Harbor, ME, USA) and maintained in a temperature/humidity controlled SPF facility with a 12 hour light/dark cycle. *Plasmodium berghei* isolate NK65 was obtained from MR4 (Malaria research and Reference Resource Center, Monassas, VA, USA). Erythrocytic stages of *P. berghei* were harvested from infected donor mice via cardiac puncture and diluted in RPMI 1640 media (ATCC, Monassas, VA, USA) supplemented with 20% heat inactivated FBS (Atlanta Biologicals, Atlanta, GA, USA). Recipient mice were infected with 2×10^7 infected erythrocytes, 200 μ L IP injection, 24 hours prior to receiving the first drug dose. Tail vein bleeds and weighing were performed daily for the duration of the experiment. All infected mice were screened prior to receiving drug or vehicle to verify an established minimum infection of 0.1% parasitemia. Inhibition of parasite growth is determined microscopically by staining a thin smear of blood obtained from the test animal using a Wright-Giemsa stain (Fisher Scientific, Houston, TX, USA). **16** was dosed in mice orally with vehicle or with 50 mg/kg/dose 1 \times daily for 4 consecutive days. The parasite blood levels were evaluated and compared to the chloroquine control.

Molecular Modeling

Structures were displayed using the graphics program PyMol (DeLano, W. L. The PyMOL Molecular Graphics System (2002) on World Wide Web <http://www.pymol.org>).

Chemistry: General Methods—If not otherwise specified, reagents and solvents were obtained from commercial suppliers and were used without further purification. The reaction progress was monitored by thin layer chromatography (TLC) using silica gel 60 F-254 (0.25 mm) plates. Visualization was achieved with UV light and iodine vapor. Flash chromatography was carried out with silica gel (32–63 μ M). The procedures for all the synthesized compounds have been provided along with relevant literature and their discussion as illustrated in the Schemes 1–3. 7-Chloro-5-methyl-[1,2,4]triazolo[1,5-*a*]pyrimidine (**12**) was synthesized as per the previously reported procedure.²⁹ All aromatic amines or amides used in the reactions were obtained from commercial sources except naphthamide, which was synthesized according to the documented procedure.⁵¹

Analysis—¹H NMR spectra were recorded on dilute solutions in CDCl₃ or DMSO-*d*₆ or MeOD-*d*₄ at 300 MHz. Chemical shifts (δ) are reported in ppm relative to TMS and coupling constants (*J*) are reported in Hz. Spin multiplicities are described as s (singlet), brs (broad singlet), d (doublet), t (triplet), q (quartet) and m (multiplet). Electrospray ionization mass spectra (ESI-MS) were acquired on a Bruker Esquire liquid chromatograph-ion trap (LC-MS) mass spectrometer. Melting points (Pyrex capillary) were determined on a Mel-Temp apparatus and are not corrected. High resolution mass spectrometry (FABHRMS) data were obtained on JEOL HX-110 mass spectrometer for compound **16**. Purity for all compounds in Table 1 was assessed by LC-MS. Chromatography was performed on a ZorbaxExtend C18 (80A) column using buffer A (water/5% acetonitrile/1% acetic acid) and buffer B (acetonitrile/1% acetic acid) with a 20 min gradient from 20–100% buffer B, or on an Agilent Exclipse XDB-C18 5 mm (dimensions 4.6 \times 150 mm) using acetonitrile/water (0.1% formic acid), and a step gradient of 20%, 50%, 90% acetonitrile at 0, 10, 20 min respectively. Absorbance was monitored at 254 nm. Compound purity was confirmed to be >95% with the exception of compounds **5**, **7** and **15** where purity was determined to be 86–90%. Given the poor activity of these compounds they were not of interest for further development and as the results would not be impacted by the marginal improvement in purity to bring them to 95%, additional purification was not performed.

Amide Mimics

General Procedure

To a suspension of Pd(OAc)₂ (67 mg, 0.30 mmol), BINAP (185 mg, 0.30 mmol) and sodium *tertiary* butoxide (2.8 g, 29.70 mmol) in anhydrous toluene (25 mL), was added 7-chloro-5-methyl-[1,2,4]triazolo[1,5-*a*]pyrimidine (**17**) (1 g, 5.93 mmol) and then aromatic amides [4-(trifluoromethyl)benzamide (1.3 g, 6.56 mmol) and benzamide (0.8 g, 6.54 mmol)]. The reaction mixture was stirred for 24 h at 120 °C and the reaction was monitored by LC/MS until no starting material remained. The mixture was then filtered and the residue was washed with dichloromethane (2 \times 10 mL). The dichloromethane parts were dried over anhydrous sodium sulfate and subsequently concentrated *in vacuo*. The crude material was purified by flash column chromatography (on silica-gel with Ethyl acetate:hexane :: 3:2) to afford the adducts [**4** (646 mg, 43%) and **5** (918 mg, 48%)] as white solids.

N-(5-methyl-[1,2,4]triazolo[1,5-*a*]pyrimidin-7-yl)benzamide (**4**)

Mp (°C): 201. ¹H NMR (300 MHz, MeOD-*d*₄) δ (ppm): 8.50 (s, 1H), 8.09 (s, 1H), 8.06 (m, 1H), 8.03 (s, 1H), 7.74-7.59 (m, 3H), 2.72 (s, 3H). ESI-MS (*m/z*): 254.0 (M⁺).

N-(5-methyl-[1,2,4]triazolo[1,5-*a*]pyrimidin-7-yl)-4-trifluoromethylbenzamide (**5**)

Mp (°C): 187. ¹H NMR (300 MHz, MeOD-*d*₄) δ (ppm): 8.51 (s, 1H), 8.24 (d, 2H, *J* = 8.1 Hz), 8.07 (s, 1H), 7.94 (d, 2H, *J* = 8.1 Hz), 2.74 (s, 3H); ESI-MS (*m/z*): 320.1 (M[−]) [ionizes better in negative mode].

Imidazo[1,2-*a*]pyrimidine derivatives

General Procedure. 5-Hydroxy-7-methylimidazo[1,2-*a*]pyrimidine (**20a**)

A solution of 2-aminoimidazole hemisulfate (**19a**) (1 g, 7.58 mmol) and ethyl acetoacetate (1.48 g, 11.37 mmol) in glacial acetic acid (15 mL) was refluxed for 25 h. Upon cooling and subsequent evaporation of the excess liquid under suction, a light brownish solid was obtained, filtered, washed with dichloromethane several times and dried under vacuum to give the product **20a** (0.790 g, 70%).

Mp (°C): 242. ¹H NMR (300 MHz, DMSO-*d*₆) δ (ppm): 7.58 (d, 1H, *J* = 2.4 Hz), 7.36 (d, 1H, *J* = 2.4 Hz), 5.76 (s, 1H), 2.26 (s, 1H); ESI-MS (*m/z*): 150.1 (M⁺).

5-Chloro-7-methylimidazo[1,2-*a*]pyrimidine (**20a**)

A mixture of the hydroxy-intermediate **20a** (0.790 g, 5.30 mmol) and phosphorus oxychloride (14 mL, 150.10 mmol) formed a clear red solution upon refluxing for 2 h. The excess phosphorus oxychloride was removed *in vacuo* and the residue was precipitated using dichloromethane. The precipitates were filtered, washed several times with dichloromethane and dried under vacuum to yield the chlorinated intermediate **21a** (577 mg, 65%), which was used without purification for subsequent steps.

7-Methyl-*N*-(naphthalen-2-yl)imidazo[1,2-*a*]pyrimidin-5-amine (**6**)⁵²

2-aminonaphthalene (490 mg, 3.42 mmol) was added to a well-stirred solution of **21a** (522 mg, 3.12 mmol) in excess of absolute ethanol. The reaction mixture was heated intermittently yielding a clear solution. Stirring was then continued overnight at ambient temperature. Excess ethanol was removed by evaporation and the crude product was subjected to flash chromatographic purification (on silica-gel with dichloromethane:methanol:ammonium hydroxide :: 240:3:2) to yield **6** (546 mg, 70%). Mp (°C) > 250. ¹H NMR (300 MHz, DMSO-*d*₆) δ (ppm): 7.98-7.91 (m, 5H), 7.62-7.41 (m, 4H), 5.72 (s, 1H), 2.31 (s, 3H); ESI-MS (*m/z*): 276.1 (M⁺).

7-Methyl-*N*-(4-(trifluoromethyl)phenyl)imidazo[1,2-*a*]pyrimidin-5-amine (**16**)⁵³

To a well-stirred solution of **21a** (522 mg, 3.12 mmol) in excess absolute ethanol, was added 4-(trifluoromethyl)aniline (552 mg, 3.42 mmol) with intermittent heating yielding a clear solution. Stirring was then continued for 24 h at room temperature, excess ethanol removed by evaporation and the crude product purified by flash chromatography (on silica-gel with dichloromethane:methanol:ammonium hydroxide :: 240:3:2) to yield **16** (555 mg, 65%). Mp (°C): 292. ¹H NMR (300 MHz, DMSO-*d*₆) δ (ppm): 7.74 (d, 1H, *J* = 1.5 Hz), 7.67 (d, 2H, *J* = 8.7 Hz), 7.35 (d, 1H, *J* = 1.8 Hz), 7.26 (d, 2H, *J* = 8.4 Hz), 5.88 (s, 1H), 2.24 (s, 3H); ESI-MS (*m/z*): 293.2 (M⁺).

7-Methyl-*N*-(naphthalen-2-yl)-[1,2,4]triazolo[1,5-*a*]pyridin-5-amine (**7**)

General Procedure. To a suspension of Pd(OAc)₂ (16.75 mg, 0.075 mmol), BINAP (46.44 mg, 0.075 mmol) and sodium *tertiary* butoxide (715 mg, 7.45 mmol) in 20 mL anhydrous toluene, was added 5-Chloro-7-methyl-[1,2,4]triazolo[1,5-*a*]pyridine (**18**, commercially obtained) (250 mg, 1.49 mmol) and then 2-amino naphthalene (235 mg, 1.64 mmol). The reaction mixture was refluxed for 24 h, subsequently cooled to room temperature and then concentrated *in vacuo*. The crude material was purified by flash column chromatography (on silica-gel using ethyl acetate:hexane :: 3:2) to afford **7** (172 mg, 42%) as creamish white solid. Mp (°C): 154. ¹H NMR (300 MHz, CDCl₃) δ (ppm): 8.41 (s, 1H); 7.97-7.82 (m, 4H), 7.73 (s, 1H), 7.61-7.45 (m, 3H), 7.17 (s, 1H), 6.60 (s, 1H), 2.46 (s, 3H). ESI-MS (*m/z*): 275.2 (M⁺).

Pyrazolo[1,5-*a*]pyrimidine

General Procedure. 7-Hydroxy-5-methylpyrazolo[1,5-*a*]pyrimidine (**20b**)

A mixture of 1*H*-pyrazol-5-amine (**19b**) (1.66 g, 20.00 mmol) and ethyl acetoacetate (2.7 mL, 2.8 g, 22.00 mmol) in glacial acetic acid (15 mL) was heated under reflux for 20 h. After the reaction mixture cooled, the excess acetic acid was removed *in vacuo*. The precipitated solid was then filtered, washed with ethanol and dried under vacuum to give the **20b** (2.55 g, 85%) as white solid. Mp (°C): 295. ¹H NMR (300 MHz, DMSO-*d*₆) δ (ppm): 7.82 (s, 1H), 6.10 (s, 1H), 5.56 (s, 1H), 2.28 (s, 3H); ESI-MS (*m/z*): 150.1 (M⁺).

7-Chloro-5-methylpyrazolo[1,5-*a*]pyrimidine (**21b**)

A solution of phosphorus oxychloride (2.0 mL, 21.40 mmol) and **20b** (149 mg, 1.00 mmol) was heated under reflux for 40 minutes. The reaction mixture was then brought to room temperature, excess reagent removed *in vacuo* and the residue triturated with ice-water. The chlorinated product was extracted from the aqueous mixture using dichloromethane. The organic layer was separated, dried over anhydrous sodium sulfate and then filtered. The filtrate was concentrated and purified by flash chromatography (silica-gel with ethyl acetate:hexane :: 3:2) to afford **21b** (75 mg, 45%). Mp (°C): 38. ¹H NMR (300 MHz, CDCl₃) δ (ppm): 8.18 (s, 1H), 6.87 (s, 1H), 6.69 (s, 1H), 2.62 (s, 3H); ESI-MS (*m/z*): 168.5 (M⁺).

5-Methyl-*N*-(naphthalen-2-yl)pyrazolo[1,5-*a*]pyrimidin-7-amine (**8**)⁵²

2-amino naphthalene (57 mg, 0.40 mmol) was added to the stirred solution of **21b** (60 mg, 0.36 mmol) dissolved in absolute ethanol (20 mL). Stirring was then continued for 8 h at room temperature. Excess ethanol was removed by evaporation and the crude product was subjected to flash chromatographic purification (on silica-gel using dichloromethane:methanol:ammonium hydroxide :: 100:1:1) to yield **7** in quantitative yields (77 mg, 78%). Mp (°C): 136. ¹H NMR (300 MHz, DMSO-*d*₆): δ 10.01 (brs, NH exchangeable), 8.16 (s, 1H), 8.04-7.93 (m, 4H), 7.66-7.62 (m, 1H), 7.59-7.48 (m, 2H), 6.43 (s, 1H), 6.34 (s, 1H), 2.38 (s, 3H); ESI-MS (*m/z*): 275.1 (M⁺).

Triazolo[4,3-*b*]pyridazine

General Procedure. 8-Hydroxy-6-methyl-[1,2,4]triazolo[4,3-*b*]pyridazine (**20c**)

A well-stirred mixture of 4*H*-1,2,4-triazol-4-amine (500 mg, 5.95 mmol) and ethyl acetoacetate (1.16 g, 8.93 mmol) in glacial acetic acid (20 mL) was refluxed at 170 °C for 4 h. The reaction mixture was brought to room temperature and excess solvent evaporated. The residue was filtered using dichloromethane and was recrystallized from aqueous acetic acid to give **20c** as white solid (750 mg, 84%). Mp (°C): 306. ¹H NMR (300 MHz, DMSO-*d*₆) δ (ppm): 9.42 (s, 1H, -OH), 6.36 (s, 1H), 2.41 (s, 3H); ESI-MS (*m/z*): 151.1 (M⁺).

8-Chloro-6-methyl-[1,2,4]triazolo[4,3-*b*]pyridazine (**21c**)

A well-stirred solution of **20c** (500 mg, 3.34 mmol) in phosphorus oxychloride (10 mL, 107.01 mmol) was refluxed for 45 minutes. After completion, the reaction mixture was concentrated *in vacuo* to give a red residue, which was precipitated using dichloromethane to give **21c** (340 mg, 62%). The chlorinated intermediate was used for the subsequent step in the crude form. Mp (°C): 181.

6-Methyl-*N*-(naphthalen-2-yl)-[1,2,4]triazolo[4,3-*b*]pyridazin-8-amine (**11**)

To a suspension of Pd(OAc)₂ (22.65 mg, 0.10 mmol), BINAP (62.78 mg, 0.10 mmol) and sodium *tertiary* butoxide (968 mg, 10.00 mmol) in anhydrous toluene (20 mL), was added

20c (340 mg, 2.02 mmol) and then 2-naphthyl amine (318 mg, 2.22 mmol). The mixture was stirred overnight at 120 °C and then concentrated *in vacuo*. The crude material was purified by flash column chromatography (on silica-gel with ethyl acetate:hexane ::11:9] to afford **11** (252 mg, 45%) as white solid. Mp (°C): 195. ¹H NMR (300 MHz, DMSO-*d*₆) δ (ppm): 10.10 (brs, NH exchangeable), 9.44 (s, 1H), 8.00-7.91 (m, 4H), 7.67-7.63 (m, 1H), 7.56-7.46 (m, 2H), 6.60 (s, 1H), 2.38 (s, 3H). ESI-MS (*m/z*): 276.2 (M⁺).

Purine analogs

General Procedure. 4-(Methylethoxymethylene)-aminoimidazole-5-carboxamide (**23a**)

A mixture of 5-amino-1*H*-imidazole-4-carboxamide hydrochloride (**22a**) (1g, 6.15 mmol), triethylorthoacetate (2 mL, 10.98 mmol) in anhydrous *N,N*-dimethyl formamide (5 mL) was heated under reflux at 180 °C for 15 minutes yielding a clear solution that was cooled. Excess solvent was removed under suction and the filtration provided **23a** as light brown solid (0.949 g, 80%). Mp (°C): 248. ¹H NMR (300 MHz, DMSO-*d*₆) δ (ppm): 12.6 (brs, NH exchangeable), 7.56 (s, 1H), 7.31 (s, 2H, -CONH₂), 4.16 (q, 2H), 2.29 (s, 3H), 1.28 (t, 3H); ESI-MS (*m/z*): 197.1 (M⁺).

2-Methylhypoxanthine (**24a**)

Intermediate **23a** (1 g, 5.11 mmol) was heated at 200 °C for 30 minutes and the product was recrystallized from water to afford **24a** (612 mg, 80%) as greyish solid. Mp (°C): > 300. ¹H NMR (300 MHz, DMSO-*d*₆) δ (ppm): 13.10 (brs, NH exchangeable), 12.15 (s, 1H, -OH), 8.12 (s, 1H), 2.35 (s, 3H); ESI-MS (*m/z*): 151.2 (M⁺).

6-Chloro-2-methyl-9*H*-purine (**25a**)

N,N-dimethylaniline (3.3 mL, 26.07 mmol) was added to a suspension of **24a** (1g, 6.67 mmol) in phosphorus oxychloride (15 mL, 214.00 mmol) and the reaction mixture was refluxed for 1 h. Excess reagent was distilled off under reduced pressure and the syrupy residue was poured onto finely crushed ice. The aqueous solution was extracted with diethyl ether in order to remove *N,N*-dimethyl aniline. The ethereal solution was washed 3–4 times with cold water, dried over anhydrous sodium sulfate and distilled to afford **25a** (728 mg, 65%) [Best results were obtained using sufficient volume of ether and rapidly extracting it with cold water].

Purine analogs (**9**, **12–15**). General Procedure

Aromatic amines [2-aminonaphthalene (186.86 mg, 1.31 mmol), 2-aminoanthracene (252.10 mg, 1.31 mmol), 3-aminoquinoline (188.16 mg, 1.39 mmol), 6-aminoquinoline (188.16 mg, 1.39 mmol) and 3-amino-1*H*-pyrazole-4*H*-carbonitrile (140.92 mg, 1.30 mmol)] were added to a well-stirred solution of **25a** (200 mg, 1.186 mmol) in absolute ethanol (20 mL) and stirring was continued for 15–18 h at ambient temperature. Excess of ethanol was removed by evaporation and the crude product were purified *via* recrystallization technique to afford 2-methyl-*N*-(naphthalen-2-yl)-9*H*-purin-6-amine (**9**; yield: 246 mg, 75%), *N*-(anthracen-2-yl)-2-methyl-9*H*-purin-6-amine (**12**; yield: 310 mg, 80%), *N*-(2-methyl-9*H*-purin-6-yl)quinolin-3-amine (**13**; yield: 257 mg, 78%), *N*-(2-methyl-9*H*-purin-6-yl)quinolin-6-amine (**14**; yield: 263 mg, 80%) and 3-(2-methyl-9*H*-purin-6-ylamino)-1*H*-pyrazole-4-carbonitrile (**15**; yield: 195 mg, 68%) [Recrystallization solvents ^o ethanol (for **9** & **12**) and dichloromethane:methanol ^o 2:1 (for **13–15**)].

2-Methyl-*N*-(naphthalen-2-yl)-9*H*-purin-6-amine (9)⁵²

Mp (°C) > 300. ¹H NMR (300 MHz, DMSO-*d*₆) δ (ppm): 10.45 (brs, NH exchangeable), 8.54 (s, 1H), 8.43 (s, 1H), 7.94-7.87 (m, 4H), 7.54-7.42 (m, 2H), 2.64 (s, 3H); ESI-MS (*m/z*): 276.2 (M+).

***N*-(Anthracen-2-yl)-2-methyl-9*H*-purin-6-amine (12)**

Mp (°C) > 320 (decomp). ¹H NMR (300 MHz, DMSO-*d*₆) δ (ppm): 11.95 (bs, NH exchangeable), 8.85 (s, 1H), 8.71 (s, 1H), 8.65-8.52 (m, 2H), 8.21-7.93 (m, 4H), 7.65-7.43 (m, 2H), 2.79 (s, 3H); ESI-MS (*m/z*): 326.1 (M+).

***N*-(2-Methyl-9*H*-purin-6-yl)quinolin-3-amine (13)**

Mp (°C) 290. ¹H NMR (300 MHz, DMSO-*d*₆) δ (ppm): 11.98 (brs, NH exchangeable), 9.43 (s, 1H), 9.07 (s, 1H), 8.63 (s, 1H), 8.07-8.05 (m, 2H), 7.78-7.67 (m, 2H), 2.71 (s, 3H); ESI-MS (*m/z*): 277.1 (M+).

***N*-(2-Methyl-9*H*-purin-6-yl)quinolin-6-amine (14)**

¹H NMR (300 MHz, DMSO-*d*₆) δ (ppm): 10.29 (brs, NH exchangeable), 8.98 (m, 1H), 8.92 (s, 1H), 8.73 (d, 1H, *J* = 8.1 Hz), 8.53 (s, 1H), 8.44 (m, 1H), 8.19 (d, 1H, *J* = 8.7 Hz), 7.77 (m, 1H), 2.70 (s, 3H, CH₃). ESI-MS (*m/z*): 277.2 (M+).

3-(2-Methyl-9*H*-purin-6-ylamino)-1*H*-pyrazole-4-carbonitrile (15)

¹H NMR (300 MHz, DMSO-*d*₆) δ (ppm): 2.62 (s, CH₃), 8.58 (s, 1H), 8.63 (s, 1H). ESI-MS (*m/z*): 241.1 (M+).

Pyrazolo[3,4-*d*]pyrimidin-4-amine**General Procedure. 5-(Methylethoxymethylene)-aminopyrazole-4-carboxamide (23b)**

A well-stirred solution of 5-amino-1*H*-pyrazole-4-carboxamide hemisulfate (**22b**) (1 g, 5.70 mmol) and triethylorthoacetate (1.72 mL, 9.44 mmol) in 5 mL of anhydrous dimethyl formamide was heated under reflux for 1 h at 240 °C and the resulting solution was cooled. The excess solvent was removed by evaporation with subsequent filtration providing **23b** (1.38 g, 75%) as light brown solid. Mp (°C): 148 (decomp). ¹H NMR (300 MHz, DMSO-*d*₆) δ (ppm): 8.01 (s, 1H), 7.25 (d, 2H, -CONH₂), 4.25 (q, 2H), 2.21 (s, 3H), 1.35 (t, 3H); ESI-MS (*m/z*): 197.1 (M+).

4-Hydroxy-6-methyl-1*H*-pyrazolo[3,4-*d*]pyrimidine (24b)

The intermediate **23b** (1 g, 5.10 mmol) was heated at 250 °C for 2 hours and the residue was filtered using dichloromethane. The crude product was recrystallized from water to afford **24b** (535 mg, 70%) as greyish solid. Mp (°C): > 300. ¹H NMR (300 MHz, DMSO-*d*₆) δ (ppm): 7.96 (s, 1H); 2.34 (s, 3H); ESI-MS (*m/z*): 151.1 (M+).

4-Chloro-6-methyl-1*H*-pyrazolo[3,4-*d*]pyrimidine (25b)

A mixture of **24b** (500 mg, 3.33 mmol), *N,N*-dimethylaniline (1.7 mL) and phosphorus oxychloride (8 mL) was refluxed for 1 h till all the solid went into solution. The excess reagent was distilled under reduced pressure and the syrupy residue was poured slowly, with vigorous stirring, onto finely crushed ice. The mixture was allowed to stand for 20 minutes and the aqueous suspension was extracted with ether. The ethereal extract was washed well with water. After drying the extract over anhydrous sodium sulfate, the organic layer was distilled to yield chlorinated adduct **25b** (392 mg, 70%) as yellow powder, used in this form for subsequent step.

6-Methyl-*N*-(naphthalen-2-yl)-1*H*-pyrazolo[3,4-*d*]pyrimidin-4-amine (10)

To a well-stirred solution of **25b** (200 mg, 1.19 mmol) in 20 mL absolute ethanol, was added 2-aminonaphthalene (186.97 mg, 1.31 mmol). The stirring was continued for 12 h at ambient temperature, excess of ethanol removed by evaporation and the crude product purified *via* recrystallization using ethanol to afford **10** (133 mg, 78%) as light yellow powder. Mp (°C): > 300. ¹H NMR (300 MHz, DMSO-*d*₆): δ 8.46 (s, 1H), 7.93-8.00 (m, 5H), 7.50-7.59 (m, 2H), 2.64 (s, 3H); ESI-MS (*m/z*): 276.1 (M⁺).

Acknowledgments

The authors would like to recognize the late Dr. Ian Bathurst from Medicines for Malaria Venture (MMV) for his helpful support of the project. We also thank Drs. David Floyd and David Matthews of the (MMV) Expert Scientific Advisory Committee for helpful discussions, and Rajan K Paranjani and Martin Sadilek for analytical support. This work was supported by the United States National Institutes of Health grants R01AI53680 (to MAP and PKR) and U01AI075594 (to MAP, PKR, SAC). MAP acknowledges support of the Welch Foundation (I-1257) and PKR also acknowledges a Grand Challenge Explorations Award from the Bill and Melinda Gates Foundation. MAP holds the Carolyn R. Bacon Professorship in Medical Science and Education and the Beatrice and Miguel Elias Distinguished Chair in Biomedical Science Beatrice and Miguel Elias Distinguished Chair in Biomedical Science.

ABBREVIATIONS USED

PfDHODH	<i>Plasmodium falciparum</i> dihydroorotate dehydrogenase
PbDHODH	<i>Plasmodium berghei</i> dihydroorotate dehydrogenase
hDHODH	human dihydroorotate dehydrogenase
HTS	high throughput screening
BINAP	2,2'-bis(diphenylphosphino)-1,1'-binaphthyl
CoQ	ubiquinone
FMN	flavin mononucleotide
ACTs	Artemisinin-based combination therapies
SAR	structure activity relationships
DCIP	2,6-dichloroindophenol
TLC	thin layer chromatography
HPLC/MS	high performance liquid chromatography/mass spectrometry

REFERENCES

- Greenwood BM, Fidock DA, Kyle DE, Kappe SH, Alonso PL, Collins FH, Duffy PE. Malaria: progress, perils, and prospects for eradication. *J Clin Invest*. 2008; 118(4):1266–76. [PubMed: 18382739]
- Guerra CA, Gikandi PW, Tatem AJ, Noor AM, Smith DL, Hay SI, Snow RW. The limits and intensity of *Plasmodium falciparum* transmission: implications for malaria control and elimination worldwide. *PLoS Med*. 2008; 5(2):e38. [PubMed: 18303939]
- White NJ. Antimalarial drug resistance. *J Clin Invest*. 2004; 113(8):1084–92. [PubMed: 15085184]
- White N. Drug resistance in malaria. *British Medical Bulletin*. 1998; 54:703–715. [PubMed: 10326295]
- Olliaro P, Wells TN. The global portfolio of new antimalarial medicines under development. *Clin Pharmacol Ther*. 2009; 85(6):584–95. [PubMed: 19404247]
- Burrows JN, Chibale K, Wells TN. The state of the art in anti-malarial drug discovery and development. *Curr Top Med Chem*. 2011; 11(10):1226–54. [PubMed: 21401508]

7. Wells TN, Alonso PL, Gutteridge WE. New medicines to improve control and contribute to the eradication of malaria. *Nat Rev Drug Discov.* 2009; 8(11):879–91. [PubMed: 19834482]
8. Eastman RT, Fidock DA. Artemisinin-based combination therapies: a vital tool in efforts to eliminate malaria. *Nat Rev Microbiol.* 2009; 7(12):864–74. [PubMed: 19881520]
9. Dondorp AM, Yeung S, White L, Nguon C, Day NP, Socheat D, von Seidlein L. Artemisinin resistance: current status and scenarios for containment. *Nat Rev Microbiol.* 2010; 8(4):272–80. [PubMed: 20208550]
10. Petersen I, Eastman R, Lanzer M. Drug-resistant malaria: molecular mechanisms and implications for public health. *FEBS Lett.* 2011; 585(11):1551–62. [PubMed: 21530510]
11. Gardner MJ, Hall N, Fung E, White O, Berriman M, Hyman RW, Carlton JM, Pain A, Nelson KE, Bowman S, Paulsen IT, James K, Eisen JA, Rutherford K, Salzberg SL, Craig A, Kyes S, Chan MS, Nene V, Shallom SJ, Suh B, Peterson J, Angiuoli S, Pertea M, Allen J, Selengut J, Haft D, Mather MW, Vaidya AB, Martin DM, Fairlamb AH, Fraunholz MJ, Roos DS, Ralph SA, McFadden GI, Cummings LM, Subramanian GM, Mungall C, Venter JC, Carucci DJ, Hoffman SL, Newbold C, Davis RW, Fraser CM, Barrell B. Genome sequence of the human malaria parasite *Plasmodium falciparum*. *Nature.* 2002; 419(6906):498–511. [PubMed: 12368864]
12. Gero A, O'Sullivan W. Purines and pyrimidines in malarial parasites. *Blood Cells.* 1990; 16:467–484. [PubMed: 2257323]
13. Gutteridge W, Trigg P. Incorporation of radioactive precursors into DNA and RNA of *Plasmodium knowlesi* in vitro. *J. Protozool.* 1970; 17:89–96. [PubMed: 5420334]
14. Reyes P, Rathod P, Sanchez D, Mrema J, Rieckmann K, Heidrich H. Enzymes of purine and pyrimidine metabolism from the human malaria parasite, *Plasmodium falciparum*. *Mol. Biochem. Parasitol.* 1982; 5:275–290. [PubMed: 6285190]
15. Sherman I. Biochemistry of *Plasmodium*. *Microbiol. Reviews.* 1979; 43:453–495.
16. Jones M. Pyrimidine nucleotide biosynthesis in animals: genes, enzymes, and regulation of UMP biosynthesis. *Annu Rev Biochem.* 1980; 49:253–279. [PubMed: 6105839]
17. Nagy M, Lacroute F, Thomas D. Divergent evolution of pyrimidine biosynthesis between anaerobic and aerobic yeasts. *Proc. Natl. Acad. Sci. USA.* 1992; 89:8966–8970. [PubMed: 1409592]
18. Painter HJ, Morrissey JM, Mather MW, Vaidya AB. Specific role of mitochondrial electron transport in blood-stage *Plasmodium falciparum*. *Nature.* 2007; 446(7131):88–91. [PubMed: 17330044]
19. Goldenberg M. Leflunomide, a novel immunomodulator for the treatment of active rheumatoid arthritis. *Clinical therapeutics.* 1999; 21:1837–1852. [PubMed: 10890256]
20. Hansen M, Le Nours J, Johansson E, Antal T, Ullrich A, Loeffler M, Larsen S. Inhibitor binding in a class 2 dihydroorotate dehydrogenase causes variations in the membrane-associated N-terminal domain. *Protein Science.* 2004; 13:1031–1042. [PubMed: 15044733]
21. Herrmann M, Schleyerbach R, Kirschbaum B. Leflunomide: an immunomodulatory drug for the treatment of rheumatoid arthritis and other autoimmune diseases. *Immunopharmacology.* 2000; 47:273–289. [PubMed: 10878294]
22. Booker ML, Bastos CM, Kramer ML, Barker RH jr, Skerlj R, Bir Sdhu A, Deng X, Celatka C, Cortese JF, Guerrero Bravo JE, Krespo Llado KN, Serrano AE, Angulo-Barturen I, Belén Jiménez-Díaz M, Viera S, Garuti H, Wittlin S, Papastogiannidis P, Lin J, Janse CJ, Khan SM, Duraisingh M, Coleman B, Goldsmith EJ, Phillips MA, Munoz B, Wirth DF, Klinger JD, Wiegand R, Sybertz E. Novel inhibitors of *Plasmodium falciparum* dihydroorotate dehydrogenase with anti-malarial activity in the mouse model. *J Biol Chem.* 2010; 285(43):33054–33064. [PubMed: 20702404]
23. Deng X, Gujjar R, El Mazouni F, Kaminsky W, Malmquist NA, Goldsmith EJ, Rathod PK, Phillips MA. Structural plasticity of malaria dihydroorotate dehydrogenase allows selective binding of diverse chemical scaffolds. *J Biol Chem.* 2009; 284:26999–27009. [PubMed: 19640844]
24. Hurt DE, Widom J, Clardy J. Structure of *Plasmodium falciparum* dihydroorotate dehydrogenase with a bound inhibitor. *Acta Crystallogr D Biol Crystallogr.* 2006; 62(Pt 3):312–23. [PubMed: 16510978]

25. Liu S, Neidhardt EA, Grossman TH, Ocain T, Clardy J. Structures of human dihydroorotate dehydrogenase in complex with antiproliferative agents. *Structure*. 2000; 8(1):25–33. [PubMed: 10673429]
26. Phillips, MA.; Rathod, PK.; Baldwin, J.; Gujjar, R. Dihydroorotate dehydrogenase inhibitors with selective anti-malarial activity. WO Patent 2007149211 A1, 2007. 2007.
27. Phillips MA, Gujjar R, Malmquist NA, White J, El Mazouni F, Baldwin J, Rathod PK. Triazolopyrimidine-based dihydroorotate dehydrogenase inhibitors with potent and selective activity against the malaria parasite, *Plasmodium falciparum*. *J Med Chem*. 2008; 51:3649–3653. [PubMed: 18522386]
28. Baldwin J, Michnoff CH, Malmquist NA, White J, Roth MG, Rathod PK, Phillips MA. High-throughput screening for potent and selective inhibitors of *Plasmodium falciparum* dihydroorotate dehydrogenase. *J Biol Chem*. 2005; 280(23):21847–21853. [PubMed: 15795226]
29. Gujjar R, Marwaha A, El Mazouni F, White J, White KL, Creason S, Shackelford DM, Baldwin J, Charman WN, Buckner FS, Charman S, Rathod PK, Phillips MA. Identification of a metabolically stable triazolopyrimidine-based dihydroorotate dehydrogenase inhibitor with antimalarial activity in mice. *J Med Chem*. 2009; 52(7):1864–72. [PubMed: 19296651]
30. Gujjar R, El Mazouni F, White KL, White J, Creason S, Shackelford DM, Deng X, Charman WN, Bathurst I, Burrows J, Floyd DM, Matthews D, Buckner FS, Charman SA, Phillips MA, Rathod PK. Lead optimization of aryl and aralkyl amine-based triazolopyrimidine inhibitors of *Plasmodium falciparum* dihydroorotate dehydrogenase with antimalarial activity in mice. *J Med Chem*. 2011; 54(11):3935–49. [PubMed: 21517059]
31. Coteron JM, Marco M, Esquivias J, Deng X, White KL, White J, Koltun M, El Mazouni F, Kokkonda S, Katneni K, Bhamidipati R, Shackelford DM, Angulo-Barturen I, Ferrer SB, Jimenez-Diaz MB, Gamo FJ, Goldsmith EJ, Charman WN, Bathurst I, Floyd D, Matthews D, Burrows JN, Rathod PK, Charman SA, Phillips MA. Structure-Guided Lead Optimization of Triazolopyrimidine-Ring Substituents Identifies Potent *Plasmodium falciparum* Dihydroorotate Dehydrogenase Inhibitors with Clinical Candidate Potential. *J Med Chem*. 2011; 54(15):5540–5561. [PubMed: 21696174]
32. Hartwig JF. Palladium-catalyzed amination of aryl halides: Mechanism and rational catalyst design. *Synlett*. 1997; 4:329–340.
33. Loones KT, Maes BU, Dommissie RA, Lemiere GL. The first tandem double palladium-catalyzed aminations: synthesis of dipyrido[1,2-a:3',2'-d]imidazole and its benzo- and aza-analogues. *Chem Commun (Camb)*. 2004; (21):2466–7. [PubMed: 15514818]
34. Urgaonkar S, Nagarajan M, Verkade JG. P[N(i-Bu)CH₂CH₂]₃N: a versatile ligand for the Pd-catalyzed amination of aryl chlorides. *Org Lett*. 2003; 5(6):815–8. [PubMed: 12633079]
35. Yin J, Buchwald SL. Palladium-catalyzed intermolecular coupling of aryl halides and amides. *Org Lett*. 2000; 2(8):1101–4. [PubMed: 10804564]
36. Kappe T. Synthesis of some new imidazo[1,2-a]pyrimidin-5(1H)-ones as potential antineoplastic agents. *J. Het. Chem*. 1995; 32(3):1003–1006.
37. Senga K, Novinson T, Wilson HR, Robins RK. Synthesis and antischistosomal activity of certain pyrazolo[1,5-a]pyrimidines. *J Med Chem*. 1981; 24(5):610–3. [PubMed: 7241518]
38. Makisumi Y. Synthesis of potential anticancer agents. 5,7-Disubstituted s-triazolo[2,3-a]pyrimidines. *Chem. Pharma. Bull*. 1961; 9:801.
39. Taddei D, Kilian P, Slawin AM, Derek Woollins J. Synthesis and full characterisation of 6-chloro-2-iodopurine, a template for the functionalisation of purines. *Org Biomol Chem*. 2004; 2(5):665–70. [PubMed: 14985806]
40. Richter E, Loeffler JE, Tahlor EC. Studies in purine chemistry. VIII. A convenient synthesis of hypoxanthines and adenines. *J. Am. Chem. Soc*. 1960; 82(12):3144–3146.
41. Robins RK, Dille KJ, Willits CH, Christensen B.E. Purines II. The synthesis of certain purines and the cyclization of several substituted 4,5-diaminopyrimidines. *J. Am. Chem. Soc*. 1953; 75:263–266.
42. Robins RK. Potential purine antagonists. I. synthesis of some 4,6-substituted pyrazolo [3,4-d]pyrimidines. *J. Am. Chem. Soc*. 1956; 78:784.

43. Steck EA, Brundage RP. Some s-triazolo[b]pyridazine. *J. Am. Chem. Soc.* 1959; 81(23):6289–6291.
44. Gujjar R, El Mazouni F, White KL, White J, Creason S, Shackelford DM, Deng X, Charman WN, Bathurst I, Burrows J, Floyd DM, Matthews D, Buckner FS, Charman SA, Phillips MA, Rathod PK. Lead-optimization of aryl and aralkyl amine based triazolopyrimidine inhibitors of Plasmodium falciparum dihydroorotate dehydrogenase with anti-malarial activity in mice. *J. Med. Chem.* 2011 in press.
45. Baldwin J, Farajallah AM, Malmquist NA, Rathod PK, Phillips MA. Malarial dihydroorotate dehydrogenase: substrate and inhibitor specificity. *J. Biol. Chem.* 2002; 277:41827–41834. [PubMed: 12189151]
46. Desjardins RE, Canfield CJ, Haynes JD, Chulay JD. Quantitative assessment of antimalarial activity in vitro by a semiautomated microdilution technique. *Antimicrob Agents Chemother.* 1979; 16(6):710–8. [PubMed: 394674]
47. Jiang L, Lee P, White J, Rathod P. Potent and selective activity of a combination of thymidine and 1843U89, a folate-based thymidylate synthase inhibitor, against Plasmodium falciparum. *Antimicrob. agents and chemotherapy.* 2000; 44:1047–1050.
48. Obach RS. Prediction of human clearance of twenty-nine drugs from hepatic microsomal intrinsic clearance data: An examination of in vitro half-life approach and nonspecific binding to microsomes. *Drug Metab Dispos.* 1999; 27(11):1350–9. [PubMed: 10534321]
49. Davies B, Morris T. Physiological parameters in laboratory animal and humans. *Pharm Res.* 1993; 10:1093–1095. [PubMed: 8378254]
50. Houston J. Utility of in vitro drug metabolism data in predicting in vivo metabolic clearance. *Biochem Pharmacol.* 1994; 47:1469–1479. [PubMed: 8185657]
51. Gaspari P, Banerjee T, Malachowski WP, Muller AJ, Prendergast GC, DuHadaway J, Bennett S, Donovan AM. Structure-activity study of brassinin derivatives as indoleamine 2,3-dioxygenase inhibitors. *J Med Chem.* 2006; 49(2):684–92. [PubMed: 16420054]
52. Phillips, MA.; Rathod, PK.; Gujjar, R.; Marwaha, AS.; Charman, SA. Dihydroorotate dehydrogenase inhibitors with selective anti-malarial activity. WO Patent 2009/082691; US Patent 20090209557. 2009.
53. Phillips, MA.; Rathod, PK.; Charman, SA.; Floyd, D.; Burrows, J.; Matthews, G.; Marwaha, A.; Gujar, R.; Coteron-Lopez, J. Antimalarial agents that are inhibitors of dihydroorotate dehydrogenase. WO 2011/041304; PCT/US2010/050532, 4/07/11. 2011.

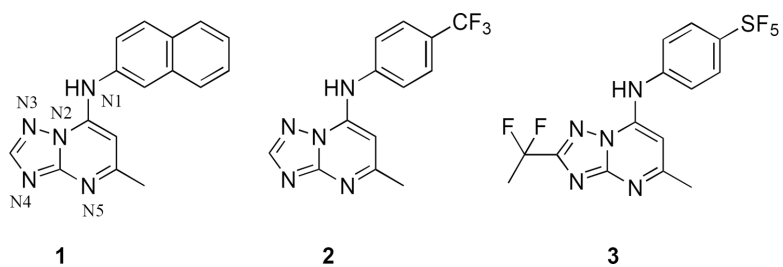


Figure 1. Triazolopyrimidines with active anti-malarial activity. The initial HTS hit (**1**), an analog with improved plasma exposure (**2**), and analog with optimized plasma exposure and potency (**3**).

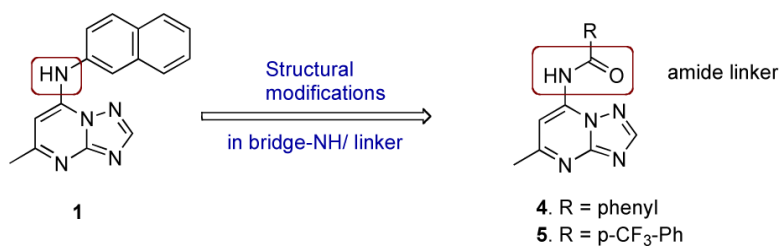


Figure 2.
Bioisosterically transformed amide mimics **4** and **5**.

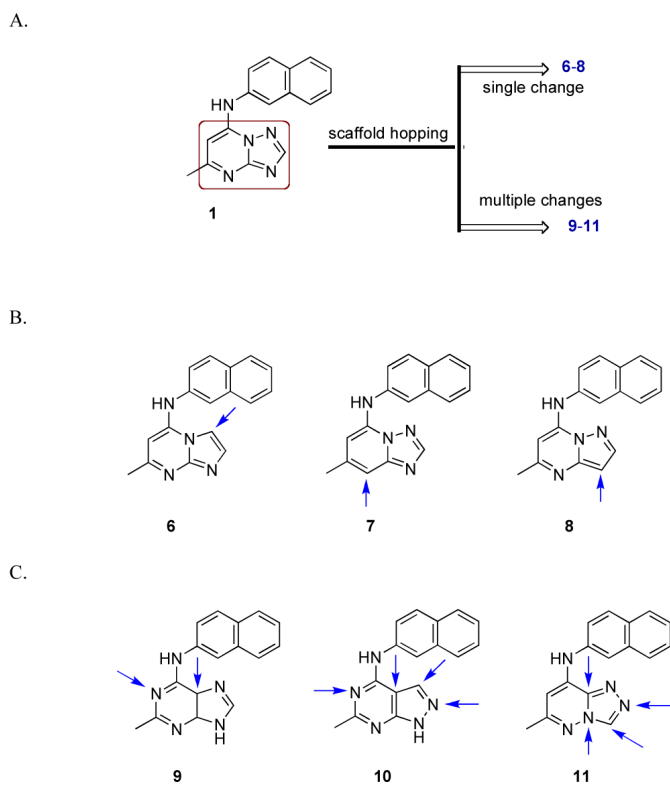


Figure 3.

A. Bioisosterically transformed scaffolds **6** – **11**. B. A virtual library comprising three types of rings with single isosteric changes in **1**. Arrows indicate the point of isosteric change. C. Various congeners with multiple isosteric changes in **1**. Arrows indicate the sites of structural diversity.

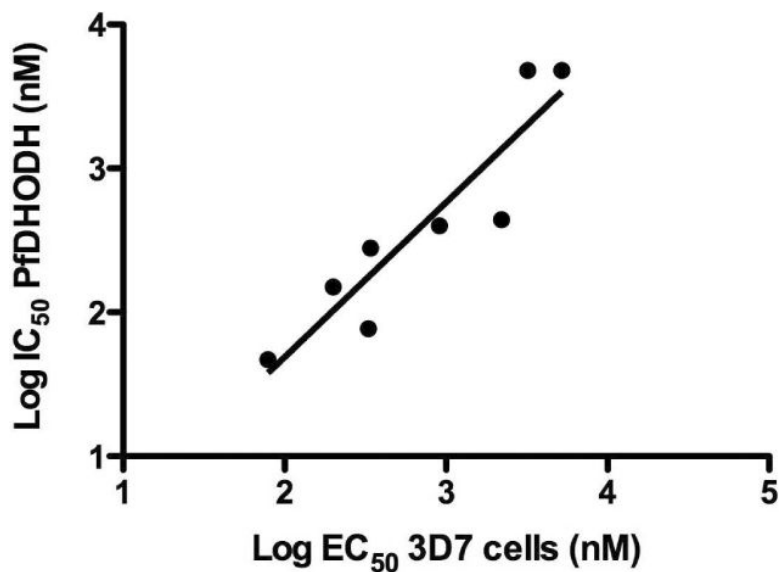


Figure 4.

Comparison of the series activity on PfDHODH vs *P. falciparum* whole cell assays. The log of the PfDHODH IC₅₀ data are plotted versus the log of the *P. falciparum* EC₅₀ data (in nanomolar). The plotted data include compounds **1**, **2**, **4–16** described in the Table 1. Compounds for which solubility limits prevented the quantitative determination of either the IC₅₀ or EC₅₀ have been left off the plot. Data were fitted by linear regression analysis where $r^2 = 0.84$ and slope = 0.93.

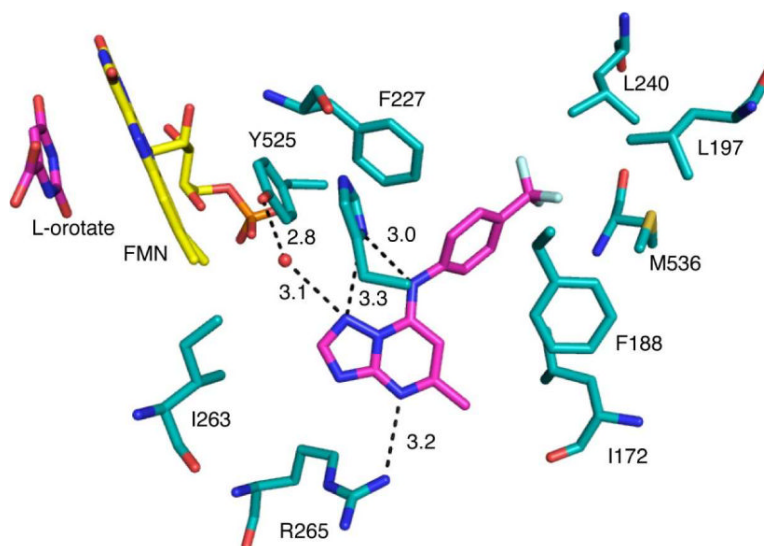
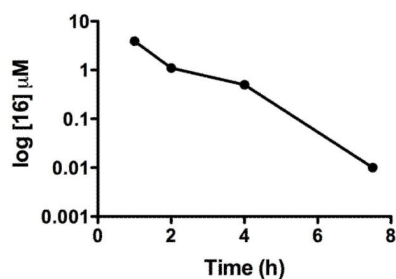
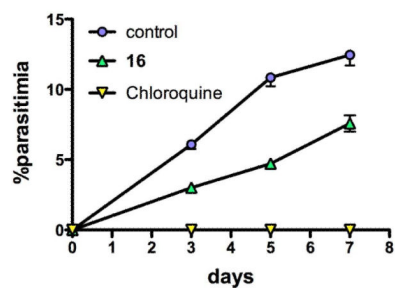


Figure 5. Binding site of **2** bound to *PFDHODH*. A limited set of residues within the 4Å shell of the bound inhibitor are displayed. **2** and orotate are displayed in pink and FMN is displayed in yellow. Hydrogen bonding distances are displayed in Å. The structure (3I6R.pdb) is displayed in PyMol.

A.



B.

**Figure 6.**

Pharmacokinetics and *in vivo* efficacy of **16** in mice. A. Pharmacokinetic profile of **16** after administration of a single oral or IP dose of 10 mg/kg. Drug concentration in micromolar is plotted versus time post dose. B. Mice were infected with *P. berghei* on day zero and **16** was dosed orally at 50 mg/kg 1 \times daily for 4 days beginning 24 h after infection. As a control chloroquine was dosed at 10 mg/kg orally using the same dosing schedule.

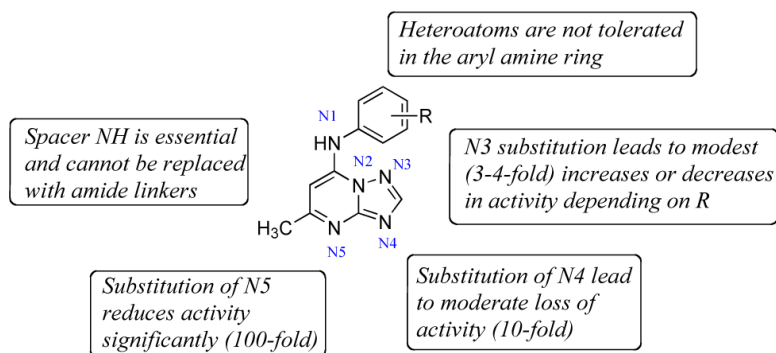
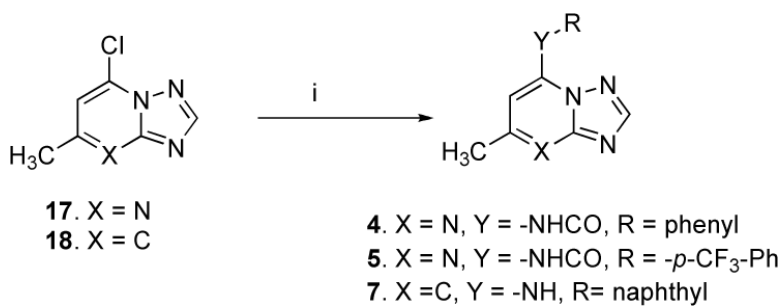
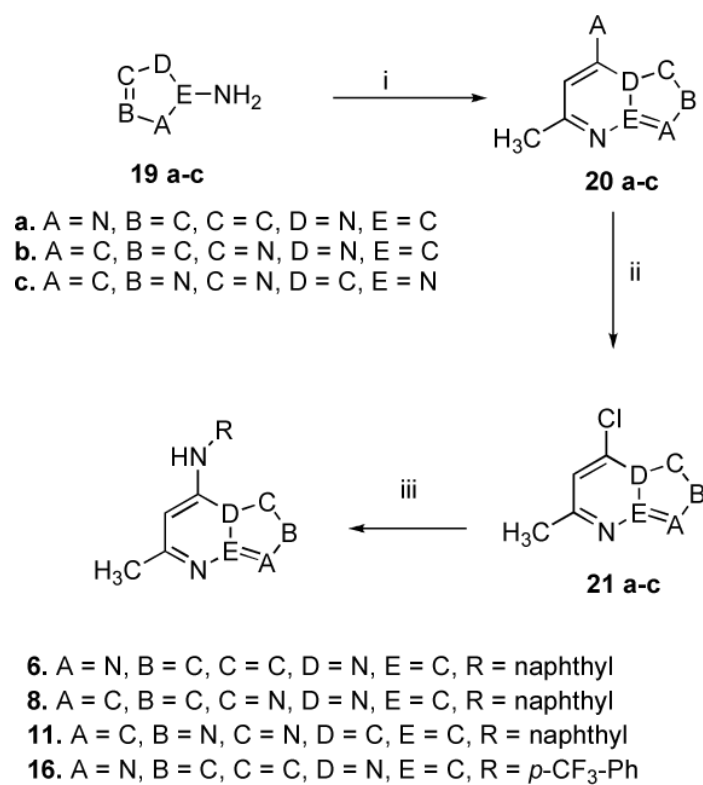


Figure 7. Structure activity map. Structural drawing of the lead core annotated to show where structural changes affect activity or potency.

**Scheme 1.**

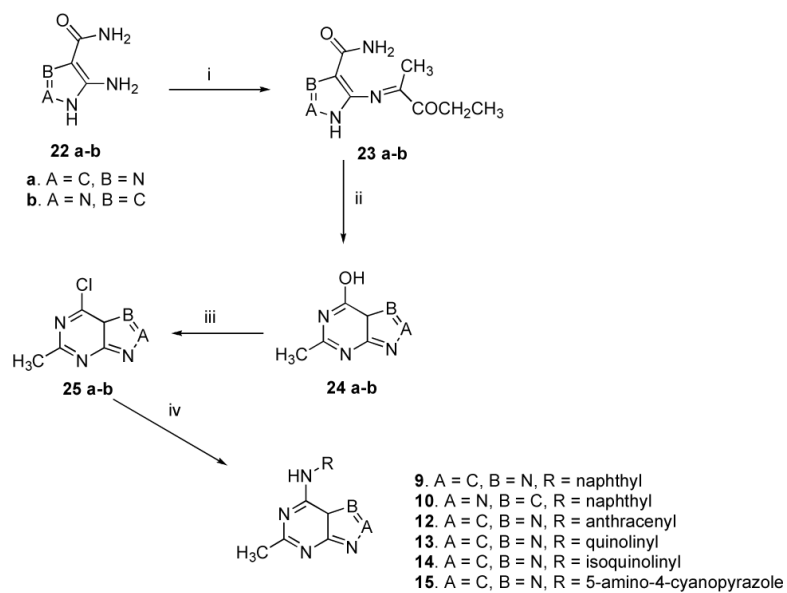
Synthetic Strategy for Inhibitors **4–5** and **7**^a

^aReagent and conditions: (i) RCONH₂ (compounds **4–5**) and RNH₂ (compound **7**), Pd(OAc)₂, BINAP NaO^tBu, anhydrous toluene, 24h reflux, yield 40–50 %

**Scheme 2.**

Synthesis of the Inhibitors **6**, **8**, **11** and **16**^a

^aReagents and conditions : (i) CH₃COCH₂CO₂C₂H₅, AcOH, reflux, 3.5–25 h, yield 70–85 %; (ii) POCl₃, reflux, 40 min–2 h, yield 60–65 %; (iii) RNH₂, EtOH, 12–18 h, room temp., yield 65–80 % (compounds **6**, **8** and **16**); Pd(OAc)₂, BINAP, NaO^t-Bu, anhydrous toluene, 24 h reflux, yield 45 % (compound **11**)

**Scheme 3.****Synthesis of Inhibitors 9, 10 and 12–15^a**

^aReagents and conditions: $\text{CH}_3\text{C}(\text{OCH}_2\text{CH}_3)_3$, anhydrous DMF, reflux, 15 min - 1 h, 70–80 %; (ii) heat above 200 °C for 1 h, yield 65–70 %; (iii) POCl_3 , 30–45 min, reflux; (iv) RNH_2 , EtOH, 15–18 h, room temp., yield 68–80 % (compounds **9–12**) and 78 % (compound **10**)

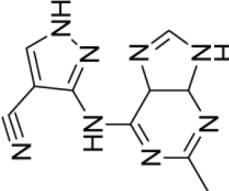
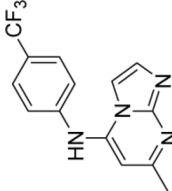
Table 1

Activity profiles of inhibitors 4–11^a

Compd	Structure	Compound code names	IC ₅₀ (μM) P/DHODH	EC ₅₀ (μM) P/3D7	IC ₅₀ (μM) hDHODH	IC ₅₀ (μM) P/hDHODH
1*		DSM1	0.047	0.076	> 100	0.23
2*		DSM74	0.28	0.34	> 100	0.38
4		DSM154	> 100	> 100	> 100	> 100

Compd	Structure	Compound code names	IC ₅₀ (μM) P/DHODH	EC ₅₀ (μM) P/3D7	IC ₅₀ (μM) hDHODH	IC ₅₀ (μM) P6DHODH
5		DSM155	> 100	> 50	> 100	> 100
6		DSM71	0.15±0.01	0.19 (0.15 – 0.25)	> 100	2.8±0.28
7		DSM96	4.8±0.7	5.2 (3.6 – 6.7)	n.d.	6.3±0.80
8		DSM68	0.4±0.09	0.91 (0.80 – 1.0)	> 100	3.3±0.4
9		DSM23	0.44±0.17	2.2 (1.2 – 3.7)	> 100	11±3.3

Compd	Structure	Compound code names	IC ₅₀ (μM) P/DHODH	EC ₅₀ (μM) P/3D7	IC ₅₀ (μM) hDHODH	IC ₅₀ (μM) P/dHODH
10		DSM70	> 100	> 12.5	n.d.	n.d.
11		DSM105	> 50	> 5	n.d.	> 50
12		DSM25	4.8±0.38	3.2 (2.4 – 3.5)	n.d.	> 10
13		DSM78	27±6.3	> 10	n.d.	n.d.
14		DSM79	>25	3.2 (2.4 – 4.3)	n.d.	n.d.

Compd	Structure	Compound code names	IC ₅₀ (μM) P7DHODH	EC ₅₀ (μM) P3D7	IC ₅₀ (μM) hDHODH	IC ₅₀ (μM) P6DHODH
15		DSM80	> 100	> 25	n.d.	n.d.
16		DSM151	0.077 ± 0.008	0.32 (0.30 – 0.35)	> 100	0.17 ± 0.018

* Data for DSM1 and DSM74 were taken from^{27,29} For enzyme data the error represents the standard error of the fit for n=3 data points per concentration; for parasite data the error displayed is the 95% confidence interval of the fit for n=3 or 4 data points per concentration.

Table 2*In vitro* metabolism in human and mouse microsomes

Compd	Degradation half-life (min)	<i>In vitro</i> CL _{int} (mL/min/mg protein)	Predicted E _H	Putative metabolites
Human				
2 *	230	0.0075	0.29	P+16
16	368	0.0047	0.21	None detected
Mouse				
16	51.8	0.034	0.59	None detected

* data were previously reported in Gujjar et al.²⁹ Data represent single point measurements.